Crowding induced morphological changes in synthetic lipid vesicles determined using smFRET

Steven D. Quinn[1,2], Jack Shepherd[1], Lara Dresser[1], Sarah Graham[1], Donato Conteduca[1] & Mark C. Leake[1,2,3]

[1]Department of Physics, University of York, York, UK. YO10 5DD.

[2]York Biomedical Research Institute, University of York, York, UK. YO10 5DD.

[3]Department of Biology, University of York, York, UK. YO10 5DD.

Correspondence to: mark.leake@york.ac.uk

Abstract:

Synthetic lipid vesicles are valuable mesoscale molecular confinement vessels for studying membrane mechanics and lipid-protein interactions, and they have found vast utility among bio-inspired technologies including drug delivery vehicles. Having a diameter of a few tens to hundreds of nanometers enables such complex processes to be studied at the level of a handful of molecules, conferring benefits in exploring molecular heterogeneity under near-physiological conditions. Vesicle morphology can be modified by changing the mixture of lipids used in creating them, fusing and lysing vesicles using proteins and detergents, or modifying the pH, temperature and ionic strength of the surrounding buffer, enabling the effects of membrane curvature on these processes to be explored. The requirements for experimental control have meant that most vesicle studies are performed under dilute solution conditions *in vitro*. The use of vesicles in crowded intracellular environments, known to influence the activities of many cellular processes, is limited by our knowledge of how molecular crowders affect vesicle morphology. To tackle this limitation, we used fluorescence spectroscopy, picosecond time correlated single photon counting and single-vesicle imaging to explore the influence of molecular crowding on the structure of freely-diffusing and surface-tethered vesicles fluorescently labelled with DiI and DiD. By quantifying single-molecule Förster resonance energy transfer (smFRET) between the probes, we determined the dependence on vesicle morphology from crowding using the molecular weight crowders sorbitol PEG400, Ficoll400 and PEG8000, identifying a common theme that both low and high molecular weight crowders trigger structural rearrangements of the vesicle that we assign to compaction. A particularly striking observation is that the low molecular weight crowder sorbitol results in irreversible changes to the smFRET efficiency attributed to permanent compaction, whereas the influence of the higher molecular weight crowders was found to be reversible. The effect of crowding perturbation on the architecture of such a reduced system not only emphasizes the power of single-vesicle approaches to probe complex biology, but also illustrates the potential to controllably alter the vesicle volume and radius of curvature for several biotechnological applications.

Keywords:

Single-molecule, TIRF, FRET, membrane mechanics, lipid vesicle, molecular crowding.

Introduction

Native biological membranes are highly complex and heterogeneous in both size and composition, which has fuelled the need for developing a range of model membrane systems that can control these physical and chemical parameters and, where appropriate, tune them[1]. A particularly valuable class of such model membranes are synthetic vesicles, spheres comprising a phospholipid bilayer surface whose composition in terms of molecular make-up can be carefully controlled resulting in diameters below the optical diffraction limit, ranging from a few tens of nanometers for small unilamellar vesicles (SUVs) to a few hundred nanometers for large unilamellar vesicles (LUVs)[2] and to up several microns for giant unilamellar vesicles (GUVs)[1]. These synthetic vesicles also offer a near physiological environment that can be tailored in terms of phospholipid composition to enable a range of localized morphologies, such as localized membrane roughness, to be achieved. Altering their composition can also result in a range of phase separation behavior across the membrane and associated differences in melting temperatures of spatially extended lipid domains. The transition temperature of the membrane is defined as the temperature necessary to promote a change in physical state from an ordered gel state to a disordered liquid crystalline state, and therefore variations in the external temperature can lead to controllable alterations of the membrane fluidity. Synthetic LUVs have thus enabled new and exciting insights into membrane mechanics[3], interactions between lipids and proteins[4,5] and the oligomerisation of encapsulated solubilised proteins such as amyloid-β peptide that aggregates *in vivo* to form amyloid fibrils[6], and the study of a range of bio-inspired drug delivery vehicles. LUVs are considered excellent candidate drug carriers because of several intrinsic advantages including biocompatibility, low toxicity, high loading capacity and controllable release kinetics[2-3]. Furthermore, inducing porosity into the membrane using bacterial toxins such as alpha haemolysin, enables buffer exchange without washing out the encapsulated biomolecules, rendering the vesicle an effective nanocontainer for allowing the interrogation of constrained biomolecules under various solution conditions[4]. Vesicles can also be biochemically programmed to fuse, enabling lipid mixing and content exchange[5-7], and the use of perturbative detergent molecules, which dramatically alter vesicle morphology[8-9], are important in the context of lysis and for triggering the release of membrane-bound or -encapsulated biomolecules[10].

The living cell's interior is a densely crowded environment, with up to 40 % of the cytoplasmic volume occupied by large solubilised macromolecules and complexes including enzymes, ribosomes and RNA[11]. In this tightly filled space, the excluded volume effect, arising from a lack of accessible space, gives rise to steric repulsions, depletion attractions, reduced translational degrees of freedom, substantial conformational changes in crowded biomolecules, and diffusional effects, all of which contribute to the chemical and biological function of the cell[12]. With this in mind, recent years have seen the development of novel experimental tools and techniques, mostly fluorescence based, for probing the effects of macromolecular crowding on protein[13-14] and nucleic acid[15-17] conformations *in vitro*. For instance, studies have seen molecular crowding modulate protein stability[18-19], biochemical interactions, reaction kinetics, diffusion[20] and liquid-liquid phase separation events[21]. These results and others not only lend support to the idea that macromolecular crowding is in itself a key regulator of biomolecular activity, but that living cells may actively regulate molecular crowding in order to enhance and adjust key biochemical processes[22]. Several different crowding mechanisms have been proposed, depending on the biomolecule and co-solute under investigation, with speculations from recent molecular dynamics studies and energy transfer experiments pointing towards an intriguing size dependence, where smaller molecular weight crowders are more effective than larger polymers[17, 23-24]. Despite such noteworthy developments, the question of how macromolecular crowding and excluded volume effects influence the behaviour and morphology of vesicles and membranes more generally remains unsettled, and thus is an area that demands further exploration.

Initially, experiments assessing the impact of macromolecular crowding on the membrane involved the use of vesicles under relatively dilute extra-vesicular concentrations of ions or other chemical factors, primarily to optimise experimental reproducibility and result in relatively low molecular crowding conditions. For example, macromolecular crowding was observed to give rise to several perturbations, including concentration- and polymer-dependent osmotic pressures, and non-specific depletions resulting from the effects of the excluded volume[25-26]. When high molecular weight crowding agents are introduced into the extravesicular space for example, the preferential exclusion of macromolecules from the membrane bilayer can introduce an osmotic imbalance which in turn alters the membrane conformation and promotes stacking and membrane fusion[27-28]. More recently, studies have shown that when crowding agents are encapsulated within lipid vesicles, depletion forces can result in membrane distortion including changes to the membrane surface area[29] and topology[30], and when highly hygroscopic crowders, such as the widely used polyethylene glycol (PEG) are used, the membrane can undergo dehydration, effectively leading to compression[31]. Optical microscopy experiments on 20-60 μm sized GUVs have also demonstrated that the encapsulation of high molecular weight PEGs induces membrane stress involving transient pulse-wise oscillations in vesicle size, changes to the global membrane tension, permeabilization and variations in the spatial orientation of membrane-bound molecules[32]. Taken together, these results support a model in which molecular crowding influences the architecture, dynamics and integrity of biological membranes. However, conventional optical microscopy experiments on GUVs, such as those reported, only reveal macroscopic changes taking place within a 2-dimensional image plane, and do not quantitatively report on molecular level changes across the 3-dimensional volume. Moreover, it is currently unclear what the influence of low molecular weight crowders are. These challenges, combined with the need to assess the structural integrity of vesicles at the opposite end of the membrane-curvature space, motivated us to extend our single-molecule Förster resonance energy transfer (smFRET) toolbox to quantitatively assess conformational changes taking place in sub-micron sized LUVs in response to the molecular crowders sorbitol, PEG 400, Ficoll400 and PEG800. Here, we showcase a high-throughput single-vesicle assay based on measuring the extent of smFRET between lipophilic membrane-integral fluorophores integrated into the membrane of LUVs to evaluate vesicle conformation in response to molecular crowding. Our approach was implemented by monitoring changes to the smFRET signal in freely-diffusing and surface-immobilized vesicles containing low concentrations of the dyes. Changes in the fluorescence signals because of crowding were monitored by ensemble-level fluorescence and picosecond time-resolved spectroscopy methods, and to explore the effect on single surface-tethered vesicles, we performed wide-field total internal reflection fluorescence (TIRF) microscopy. In particular, we find that both sorbitol, a model sugar based cosolvent for low molecular weight crowding[33], and high molecular weight crowders could be observed to induce variations in the observable FRET efficiency assigned to vesicle expansion. However, a striking observation is that whilst the compaction induced by the high molecular weight crowders was reversible, sorbitol-induced vesicle compaction was found to be permanent. We discuss the implications of our findings for enabling control over lipid vesicle size and architecture, and how this could transform future insight into a range of cellular and biotechnological processes.

Materials and Methods

Lipid vesicle preparation

1-palmitoyl-2-oleoyl-glycero-3-phosphocholine (POPC) and 1-palmitoyl-2-oleoyl-sn-glycero-3-phospho-L-serine (POPS) lipids in chloroform were purchased from Avanti Polar Lipids and used without any additional purification. 1,1'-Dioctadecyl-3,3,3',3' Tetramethylindocarbocyanine Perchlorate (DiI) and 1,1-Dioctadecyl-3,3,3,3-tetramethylindodicarbocyanine (DiD) membrane stains were obtained from ThermoFisher Scientific. Synthetic lipid vesicles were prepared via the extrusion method as previously described[8-9]. Briefly, mixtures of lipids and membrane stains as described in the main text were mixed in chloroform at typical final lipid concentrations of 10 mg lipid/ml. The solvent was then evaporated by nitrogen flow to create a dry lipid film and this was subsequently hydrated in 50 mM Tris buffer (pH 8.0) and mixed well by vortex. The resuspended solution was then extruded through a polycarbonate membrane filter of defined pore size to produce vesicles of comparable diameter.

Ensemble Fluorescence Spectroscopy

Fluorescence emission spectra obtained from freely diffusing DiI and DiD loaded vesicles in 50 mM Tris buffer (pH 8) were recorded using a HORIBA Fluoromax-4 spectrophotometer with λ_{ex} = 532 nm. All experiments were performed using a final lipid concentration of 25 µM in 50 mM Tris buffer (pH 8). Apparent FRET efficiencies, E_{FRET}, were estimated via $E_{FRET} = (I_A/[I_A+I_D])$, where I_A and I_D are the integrated, background-corrected fluorescence emission intensities of the donor, DiI, and acceptor, DiD, respectively. Data points plotted represent the mean and standard error of the mean obtained from three separated experimental runs.

Time Correlated Single Photon Counting

Time-resolved fluorescence decays were collected using a FluoTime300 time-correlated single photon counting spectrophotometer equipped with a hybrid PMT detector (Picoquant, Germany). Decays were measured under magic angle conditions using pulsed excitation of 532 nm wavelength (80 MHz) and emission of 565 nm for DiI-DiD loaded vesicles and an excitation of 485 nm (20 MHz) and emission of 600 nm for vesicles containing LIPid Tension Reporter (FliptR)[42]. All experiments were performed using a final lipid concentration of 25 µM in 50 mM Tris buffer (pH 8). Decays were acquired until 10^4 counts at the decay maximum were observed and fitted by iterative re-convolution of the instrument response function and the observed fluorescence decay using a multi-exponential decay function of the form:

$$I_t = \sum_{i=1}^{n} a_i e^{-\frac{t}{\tau_i}},$$

where I_t is the intensity at time, t, normalized to the intensity at t = 0, and t_i and a_i represent the fluorescence lifetime and fractional amplitude of the i^{th} decay component.

Dynamic Light Scattering

The mean hydrodynamic diameter, d_H, of freely diffusing vesicles at a final lipid concentration of 25 µM as a function of crowder were acquired using a Zetasizer µV system equipped with a λ_o = 632.8 nm wavelength line. Briefly, Brownian motion of LUVs in solution gave rise to fluctuations in the intensity of back scattered light at angle θ = 178° as a function of time, t, which were used to produce a correlation function, $G(\tau)$, via $G^2(\tau) = \langle I(t)I(t+\tau)\rangle / \langle I(t)^2\rangle$ where τ is the lag time. Correlation curves were fitted to a single diffusing species model of the form $G(\tau) = A[1 + Be^{-2Dq^2\tau}]$ where D is the vesicle

diffusion coefficient, *A* and *B* are positive constants and $q = \frac{4\pi n}{\lambda_o} sin\left(\frac{\theta}{2}\right)$, where *n* is the refractive index of the solution (*n*=1.33). Hydrodynamic diameters were then calculated according to the Stokes-Einstein relationship[34] and reported as the mean and standard error of the mean from three separated experimental runs.

Scanning Electron Microscopy

SEM micrographs of vesicles non-specifically bound to a silicon substrate were acquired using a JEOL JSM-7800F system operating at 5 kV as previously described[35,55]. Vesicles were prepared in 50 mM Tris buffer (pH 8) containing molecular crowders at concentration specified in the main text, diluted ~10x in deionized water and vortexed. The solution with vesicles was finally applied to the silicon substrate and then evaporated. The substrate with the remaining vesicle layer was then sputtered with a 5 nm thick Pt/Pd surface layer to avoid charging effects and possible damage of the vesicles during the micrographs acquisition. Vesicle diameters were then determined using ImageJ.

TIRF microscopy

Microfluidic flow cells were constructed and sequentially flushed and incubated with 0.1 mg/mL BSA-Biotin, 1 mg/mL BSA and 0.2 mg/mL NeutrAvdin. After each incubation step the flow cells were rinsed with buffer (50 mM Tris, pH 8) to remove unbound material. Biotinylated vesicles containing 0.1 mol % DiI and 0.1 mol% DiD were then added to the surface using a final concentration of 70 µg/mL lipids in imaging buffer (50 mM Tris, 6 % (W/V) D-(+)-glucose containing 1 mM Trolox and 6.25 µM glucose oxidase and 0.2 µM catalase) and incubated for 15 minutes at room temperature to achieve a surface coverage of ~150-200 vesicles per 50 x 50 µm field of view. After incubation, the flow cell was rinsed with imaging buffer to remove any unbound vesicles. TIRF microscopy was then performed on a custom-modified inverted microscope (Nikon Eclipse Ti) containing a CFI Apo TIRF 100 x NA 1.49 oil-immersion objective lens (Nikon). TIRF illumination was provided by a TEM_{00} 532 nm line (Obis, Coherent). Emission was separated from the excitation line via a dichroic and emission filter mounted beneath the lens turret (Chroma 59907-ET-532/640). DiI and DiD emission was then spatially separated using a DualView image splitter (Photometrics) containing a dichroic filter (T640LPXR, Chroma) and band pass filters (ET585/65M and ET700/75M, Chroma) and imaged in parallel on a back-illuminated Prime 95b CMOS camera cooled to -30°C (Photometrics). After each addition of sorbitol in imaging buffer, movies were acquired with 50 ms exposure time. Recorded images were then analysed in MATLAB (R2019a) using iSMS single-molecule FRET microscopy software[36]. Briefly, the donor and acceptor emission channels were aligned, and background-corrected DiI and DiD emission trajectories were obtained by integration of the intensity within the area containing the vesicle signal for each time point. Apparent FRET efficiencies were calculated using a similar formulation as for ensemble FRET, of $I_A/(I_A+I_D)$ where I_A and I_D are the acceptor and donor emission intensities, respectively and related to the mean distance between probes, *R*, via $E = \frac{R_0^6}{R_0^6+R^6}$, where R_o = 5.3 nm is the Förster radius.

Results and Discussion

Sorbitol induces conformational changes in freely diffusing lipid vesicles.

We first used single-molecule FRET (smFRET) between lipophilic membrane stains to explore the structure of LUVs composed of POPC lipids, which are excellent model systems for studying extracellular vesicles and biological membranes more generally, in the presence of the molecular

crowder sorbitol. Previous studies evaluating membrane deformation have largely relied on pegylated-lipids added to synthetic cells to stimulate crowding within the membrane and giant (> 5 µm) vesicles, with intensity-based single-colour fluorescence imaging used to evaluate morphology[37]. However, as we reported previously, conventional intensity-based imaging approaches can only resolve macroscopic structural changes while providing little detail on the molecular level[8]. We therefore applied the smFRET approach to quantify the packing density of single vesicles at the opposite end of the membrane curvature space, and in in particular those smaller than the optical diffraction limit (~250 nm), to follow the vesicle response to molecular crowding. The amount of donor (DiI) and acceptor (DiD) dyes on the membrane surface were optimized (1: 1 ratio, 0.1 % of each dye), such that the average FRET efficiency (E_{FRET}) per vesicle was initially close to the Förster radius, allowing length scale changes because of vesicle compaction or swelling to be quantified by an observable increase or decrease in E_{FRET}, respectively. To mimic low molecular weight crowding conditions in solution, we used the polyol osmolyte sorbitol, a well-established low molecular weight crowding agent which has previously been applied to regulate protein clustering[38-40], and induce nuclear organization and chromatin compaction[41]. We first recorded the fluorescence emission spectra obtained from freely diffusing vesicles incorporating DiI and DiD in the absence and presence of sorbitol. Dynamic light scattering confirmed the formation of fluorescently-tagged vesicles with a log-normal diameter distribution centred on a peak value of 227 nm (**Figure S1**). When vesicles were prepared without DiI and DiD, the diameter distribution was found to similar, providing confidence that the introduction of the labels does not perturb vesicle morphology (**Figure S1**). As shown in **Figure 1A,** DiI and DiD loaded vesicles displayed a progressive increase in the sensitized acceptor emission as the sorbitol concentration increased, translating to an overall increase in FRET efficiency and reduction in the mean DiI-DiD separation distance, from 5.02 ± 0.02 nm in the absence of sorbitol to 4.76 ± 0.01 nm in the presence of sorbitol at 3 M (**Figure 1B**). To further confirm the presence of an energy transfer mechanism, we measured the fluorescence lifetime of DiI in the presence of DiD via the time-correlated single photon counting (TCSPC) approach. This involved illuminating low concentrations of the labelled vesicles with pulsed laser excitation, and measuring the decay in ensemble emission intensity against time as a means to extract the amplitude weighted average lifetime, t_{av}, as described in the **Methods Section.** Here, τ_{av} progressively decreased as a function of sorbitol, consistent with a progressive quenching of DiI and corresponding increase in E_{FRET} (**Figure 1C**). We note that the fluorescence decays fitted well to a bi-exponential decay model after reconvolution with the instrumental response function, which we speculate is indicative of energy transfer on the inner and outer membrane layers. Indeed, a bootstrap analysis revealed that both lifetime components, termed τ_1 and τ_2 respectively, progressively decreased with increasing sorbitol (**Figure S2**), indicative of conformational changes on both sides of the membrane. Taking these measurements together, the data points towards fluorophore packing in the ensemble which we assigned to vesicle compaction.

To test the possibility that the POPC membrane tension was also regulated by sorbitol, we next evaluated variations in the fluorescence lifetime of the membrane tension probe Fluorescent LIPid Tension Reporter (FliptR) embedded within the vesicle bilayer. As previously demonstrated, the FliptR lifetime depends strongly on the membrane tension[42], and here, we prepared 200 nm diameter POPC vesicles incorporating ~1 mol % FliptR. We subsequently measured the dye lifetime via TCSPC and found that they were best fitted to biexponential decay models. However, in line with previous observations, the longer lifetime, τ_2, only accounted for a small fraction of the overall signal, likely due to the presence of a small degree of free dye in solution. In the absence of sorbitol the average FliptR lifetime was found to be 3.14 ± 0.01 ns, corresponding to a situation where the dyes are in a relatively planar conformation. However, with increasing levels of molecular crowding, we observed a reduction in lifetime to ~90 % of its original value (**Figure 1D, Figure S3**), which we assigned to a fraction of FliptR

molecules twisting into a conformation that is sterically more favorable because of changes to the lipid packing density and decreased membrane tension. Similar to observations made with single vesicles in response to surfactants[43], we speculated that phospholipid bilayers mixed well with sorbitol, leading to a situation where the two bilayer components were forced by entropy, resulting in mixed aggregates, local membrane undulations, and reduced membrane tension.

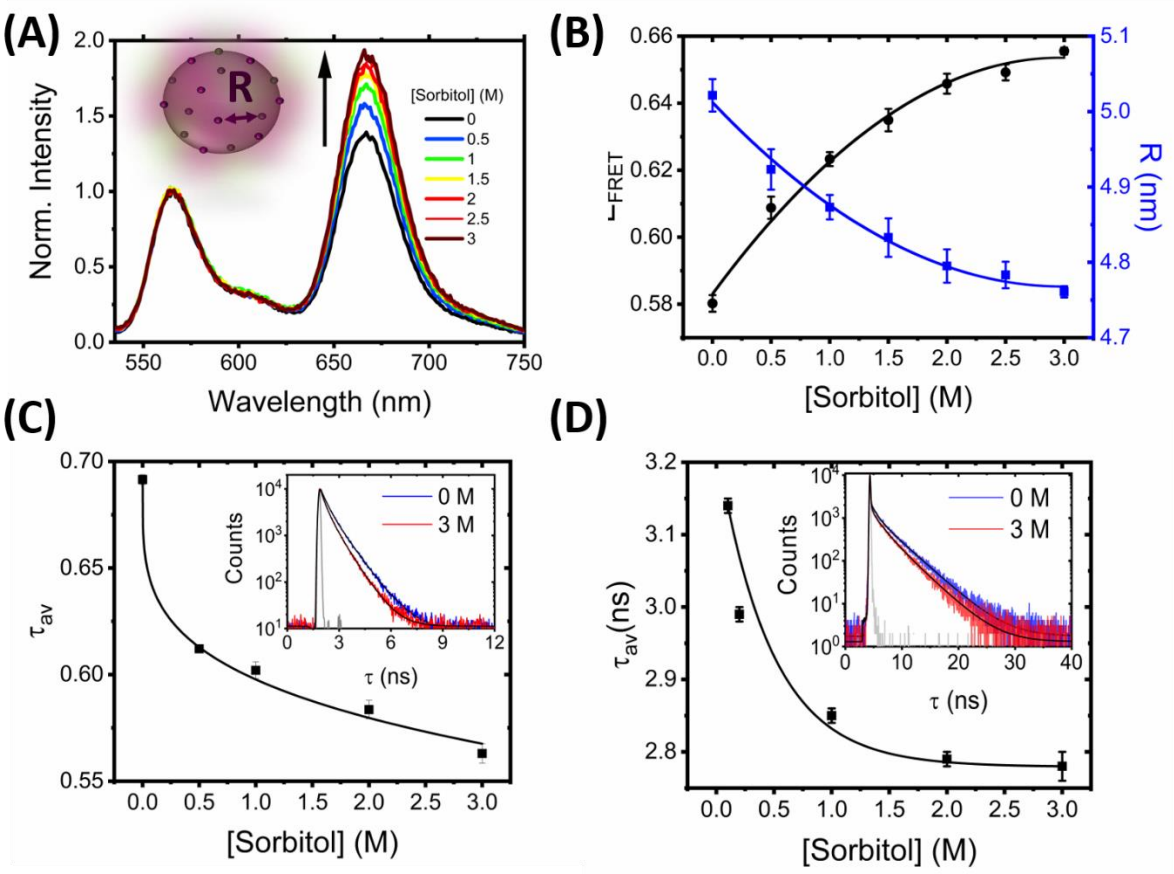

Figure 1. Sorbitol induces conformational changes in freely diffusing vesicles. (A) Normalized fluorescence emission spectra of DiI and DiD loaded 200 nm diameter vesicles in the absence and presence of sorbitol with λ_{ex} = 532 nm. Inset: schematic illustration of the vesicles, where *R* corresponds to the mean dye-dye separation distance. (B) Corresponding variations in the efficiency of energy transfer, E_{FRET}, and *R*. Heuristic fits shown are quadratic, determined with Python 3 using NumPy's polyfit routine (C) The amplitude weighted average lifetime of DiI and (D) FliptR as a function of sorbitol. Insets correspond to the time-resolved fluorescence decays in the absence (blue) and presence of 3M sorbitol (red). Solid black lines represent biexponential fits to the raw data and the solid gray lines represent the instrument response functions.

The ensemble FRET, lifetime and FliptR analysis broadly supports conformational rearrangements taking place in LUVs in response to sorbitol, however, to understand the parameters that affect this process, we next moved to interrogate the impact of vesicle size, composition and phase. When solutions of vesicles of various sizes (100, 400 and 1000 nm), as confirmed by DLS (**Figure S4**), corresponding to SUVs, LUVs and GUVs, respectively, were allowed to interact with sorbitol, the FRET efficiencies in all cases increased with sorbitol concentration, signifying similar dye-dye distance changes and comparable degrees of conformational changes (**Figure S5**). Indeed, the overall response

in terms of relative magnitude compared to those observed with 200 nm sized vesicles was similar across all conditions tested. To assess the impact of lipid composition and phase, we also probed the interaction between sorbitol and 100 nm diameter vesicles loaded with negatively charged POPS lipids as a function of temperature and compared the relative change in FRET efficiency to similarly sized vesicles composed of POPC (**Figures S5**). POPC has a gel-to-liquid phase transition temperature, T_M, of -2°C, and is therefore in the liquid phase at temperatures > 4°C whereas for POPS lipids, T_m = 14°C, below which the vesicles are in the gel phase. We observed that the initial magnitude of the FRET efficiency was similar for both sets of vesicles across the temperature range (4°C, 21°C and 37°C) investigated, however the relative change in E_{FRET} for each sorbitol condition was generally larger in the case of POPC vesicles. One possible explanation for the observed difference could rest in the hydration of the lipid carbonyls. It is well established that vesicles incorporating POPS are less mobile and dehydrated relative to the POPC forms[44], suggesting uptake of sorbitol into the bilayer may be key for conferring the observed changes in FRET efficiency.

To explore whether the observed changes in FRET efficiency were coupled with changes in vesicle morphology, we next investigated the size distributions of single vesicles in the absence and presence of sorbitol using scanning electron microscopy. As shown in **Figure 2A**, vesicles composed of POPC lipids in the absence of sorbitol were mostly spherical (circularity = 0.87 ± 0.16) in nature with a diameter centred on 132 ± 3 nm (FWHM = 125 ± 8 nm). However, with the addition of sorbitol, the size distribution peak shifted to 105 ± 5 (FWHM = 155 ± 15 nm) (**Figure 2B**) and the circularity reduced to 0.55 ± 0.12, consistent with a model in which sorbitol leads to local membrane undulations and an overall conformational change that can be assigned to compaction. Our observations of spherical vesicle morphologies in the absence of sorbitol are in line with previous observations[35]. However, when the vesicles were incubated in the presence of sorbitol, the mean dye-dye spatial separation distance reduced as confirmed via ensemble FRET measurements, leading to the compaction of intact vesicles. This analysis was further supported by variations in the mean vesicle hydrodynamic diameter (d_H) of vesicles reported by DLS **(Figure S6)**, where the mean hydrodynamic diameter of the vesicles in solution decreased upon increasing concentrations of sorbitol. We note that differences in the initial vesicle size reported by DLS differs from those reported by SEM, however, one explanation for this is the fact that vesicles are dehydrated and fixed under vacuum. Nevertheless, both measurements point to the sorbitol-induced structural remodelling of single intact vesicles, and more generally highlight the impact of molecular crowding on this important class of biomolecular system.

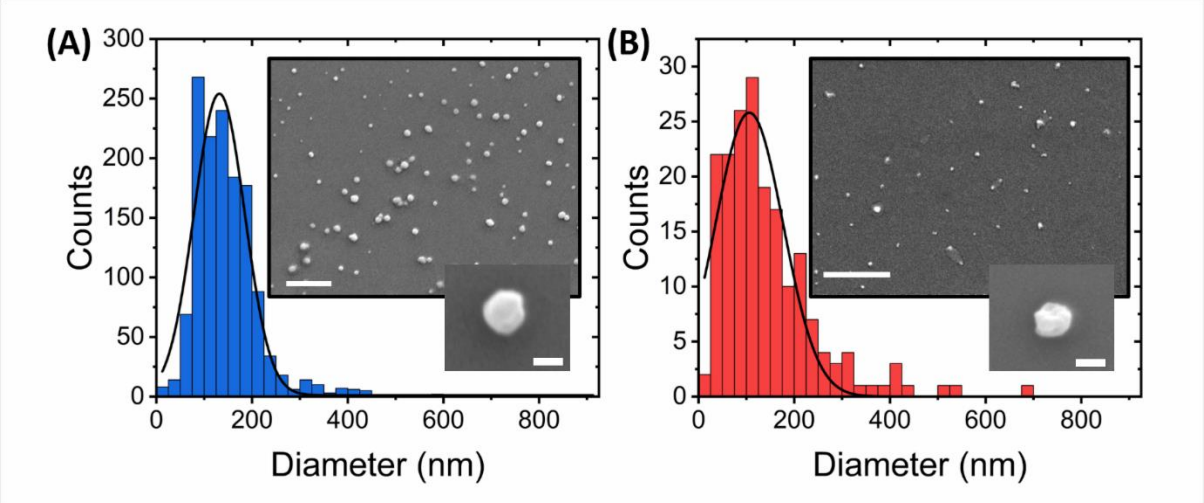

Figure 2. Sorbitol induces compaction and undulations in single lipid vesicles. Quantitative comparison of diameter distributions of POPC vesicles in (A) the absence and (B) presence of 3 M

sorbitol. Insets: representative SEM images of immobilized vesicles under the respective conditions. Scale bars = 1 µm and 100 nm in the larger and smaller insets, respectively.

Sorbitol-induced compaction of surface-tethered vesicles is irreversible

To further visualize the observed compaction event, we next evaluated the mean FRET response from single surface-tethered vesicles under crowding conditions by simultaneously capturing DiI and DiD fluorescence intensities using a custom built wide-field objective-type total internal reflection fluorescence microscope[45]. Prior to the extrusion process, the lipid suspension contained 1 mol% of Biotin-PE, allowing formed vesicles to be tethered to a glass substrate via BSA-Biotin and NeutrAvidin as previously described[9]. As shown in **Figure 3A,** the application of picomolar vesicle concentrations to a NeutrAvidin coated surface led to the detection of 195 ± 14 FRET-active vesicles per field of view (25 x 50 µm), with a mean nearest-neighbour vesicle separation distance of ~1 µm. To minimize photobleaching, the vesicles were studied under low excitation intensities and an oxygen scavenger cocktail consisting of Trolox, glucose oxidase and catalase was included in the base imaging buffer (50 mM Tris, pH 8) to prolong photostability. In the absence of sorbitol, the vesicles displayed fluorescence emission across both DiI and DiD channels, indicative of substantial FRET due to their close proximity. Interestingly, intensity distributions composed of the mean DiI and DiD fluorescence counts obtained from N = 1,566 diffraction- limited fluorescent foci displayed lognormal behaviour (**Figure 3B**), which as previous studies indicate[46-47], could represent a distribution of vesicle sizes on the surface. As sorbitol was progressively added to the vesicle layer, we then recorded variations in the FRET efficiency per vesicle via changes to the DiI and DiD emission. Here, we observed a progressive increase in relative sensitized acceptor emission as the sorbitol concentration was increased because of enhanced FRET between the dyes (**Figure 3C**). During the titration, the number of diffraction limited spots per field of view and the mean total fluorescence intensity per vesicle defined as the sum of DiI and DiD emission intensities remained largely unchanged, providing confidence that addition of sorbitol left vesicles intact on the surface. The positive shift in FRET efficiency population distribution histograms (**Figure 3D**) then observed as sorbitol was progressively titrated was not therefore attributed to partial lipid loss or photophysical artefacts, but rather to a structural alteration, namely compaction, taking place within single intact vesicles, where the mean donor-acceptor separation distance, $\langle d \rangle$ progressively reduced **(Figure 3E)**. Interestingly, this result is complementary to previous observations where encapsulated molecular crowders led to vesicle bulging in giant vesicles[32]. In contrast here, the application of low molecular weight crowders to the vesicle exterior leads to vesicle shrinkage. The effect of sorbitol on vesicle morphology appeared instantaneous on our measurement timescale and we found that the compaction process was irreversible over the measurement timescale. As shown in (**Figure 3F**), flushing the vesicle solution with sorbitol led to a shift in the FRET distribution, but there was no change thereafter when the vesicles were thoroughly washed with buffer solution, ruling out an excluded volume effect as the cause of the compaction. Instead, this observation points towards a situation where after interaction of the membrane with sorbitol, the membrane phase transition temperature is irreversibly depressed in a dose-dependent manner via an interaction that we speculate could involve sorbitol interactions with the functional phosphate groups of the lipids on the surface.

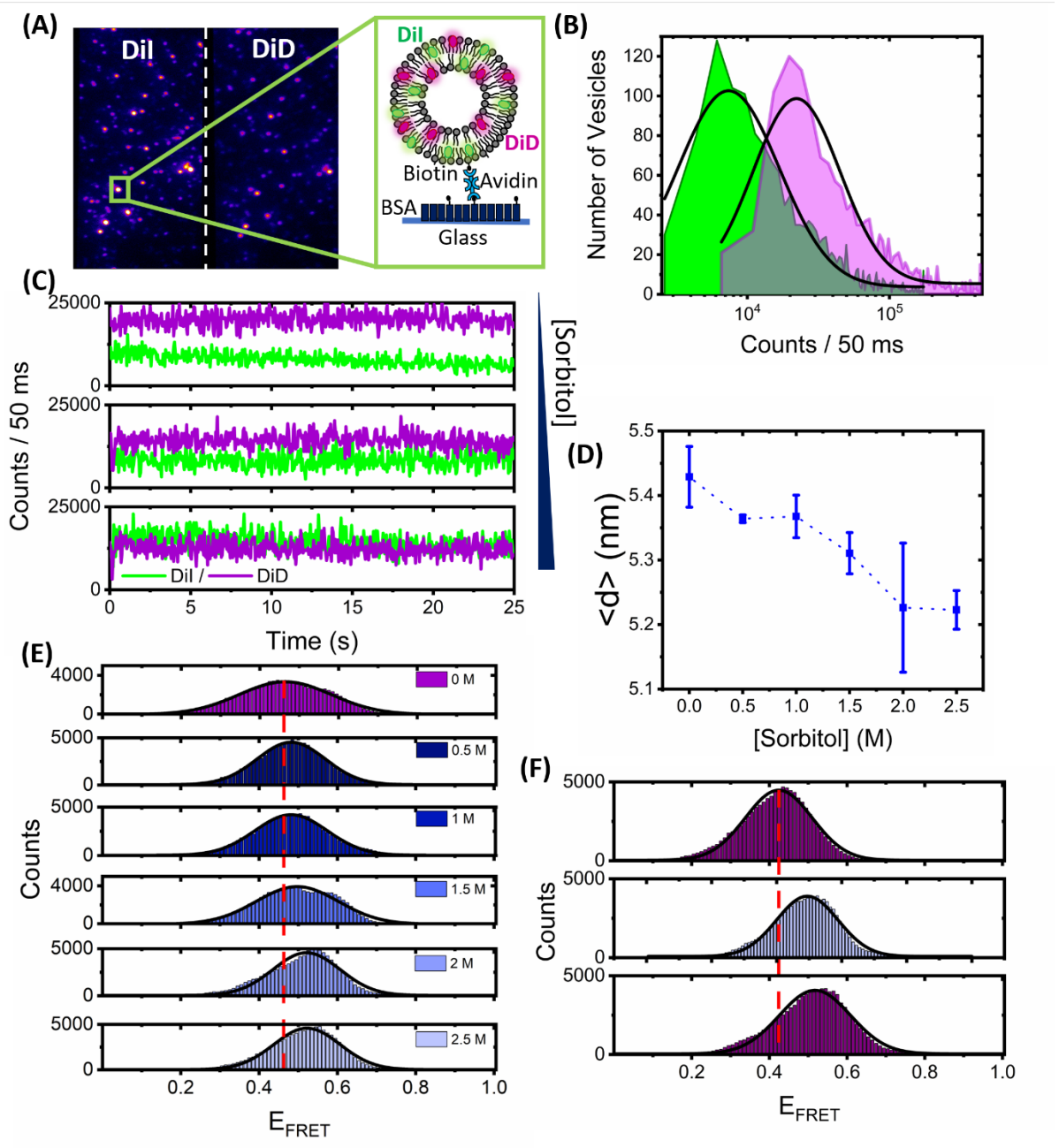

Figure 3. Sorbitol induces irreversible structural changes in single surface-tethered vesicles. (a) Representative wide-field TIRF image of surface tethered vesicles composed of DiI and DiD. Donor and acceptor emission channels are shown on the left- and right-hand side of the dashed line, respectively. Inset: surface immobilization scheme. Single vesicles containing biotinylated lipids are immobilized onto a BSA-Biotin coated glass coverslip via NeutrAvidin. (B) Fluorescence intensity population histograms of DiI (green) and DiD (magenta) obtained from surface tethered vesicles in the absence of sorbitol. (C) Representative time traces of DiI (green) and DiD (magenta) obtained from single surface tethered vesicles with 0 mM (top), 1 M and 3 M sorbitol. (D) Representative variation in the mean probe separation distance as a function of sorbitol concentration. (E) Corresponding variations in the FRET efficiency histograms obtained for N > 2,000 vesicles. (F) FRET efficiency histograms obtained from N > 2,000 vesicles at 0 mM sorbitol, after a 3 M sorbitol rinse step (middle panel), and after vigorous washing of the sample with 50 mM Tris (pH 8) buffer solution (lower panel). The dashed red lines in (E) and (F) correspond to the peak positions of the FRET efficiency histograms obtained in the absence of sorbitol. Solid black lines represent single Gaussian fits.

Having established the DiI-DiD FRET pair as a sensitive indicator of single-vesicle compaction, we next explored the effect of higher molecular weight crowding agents known to induce excluded volume effects, on vesicle morphology. Here, we also evaluated the fluorescence response of surface-immobilized LUVs tagged with DiI and DiD in response to variations of the widely used polyethyleneglycol (PEG) and Ficoll400. As has been extensively reported elsewhere, macromolecular crowding by PEG and Ficoll, even at modest concentrations of 0 - 25 %(*w/V*) in solution, can trigger significant excluded volume effects, regulate mesoscale biological functions and substantially impact the nanoscale conformations of single biomolecules[15, 48-51]. As shown in **Figure 4A**, the application of modest concentrations (5 – 20 % (*w/V*)) of PEG400, a 400 Da grade of PEG, also led to positive shifts in the population FRET efficiency histograms. It is noteworthy that Ficoll400 had a similar effect on the FRET efficiency distributions under identical working conditions (**Figure 4B**) which we interpreted as evidence that crowding by the excluded volume effect also induces morphological compaction. When a high molecular weight (8 kDa) grade of PEG, PEG8000, was introduced to the immobilized vesicles, similar observations were made, though we note the magnitude of the FRET efficiency shift at 20 % (*w/V*) crowder was more pronounced. A striking observation was that in the case of both low and high molecular weight PEG crowders, the FRET efficiency of the vesicles then recovered to lower values after the systems were thoroughly washed with buffer (**Figure 4D**), indicating that vesicle compaction by excluded volume effects are reversible. We note that this is in direct contrast to the observations made with sorbitol, where we speculate encapsulation of the crowder within the bilayer leads to irreversible compaction.

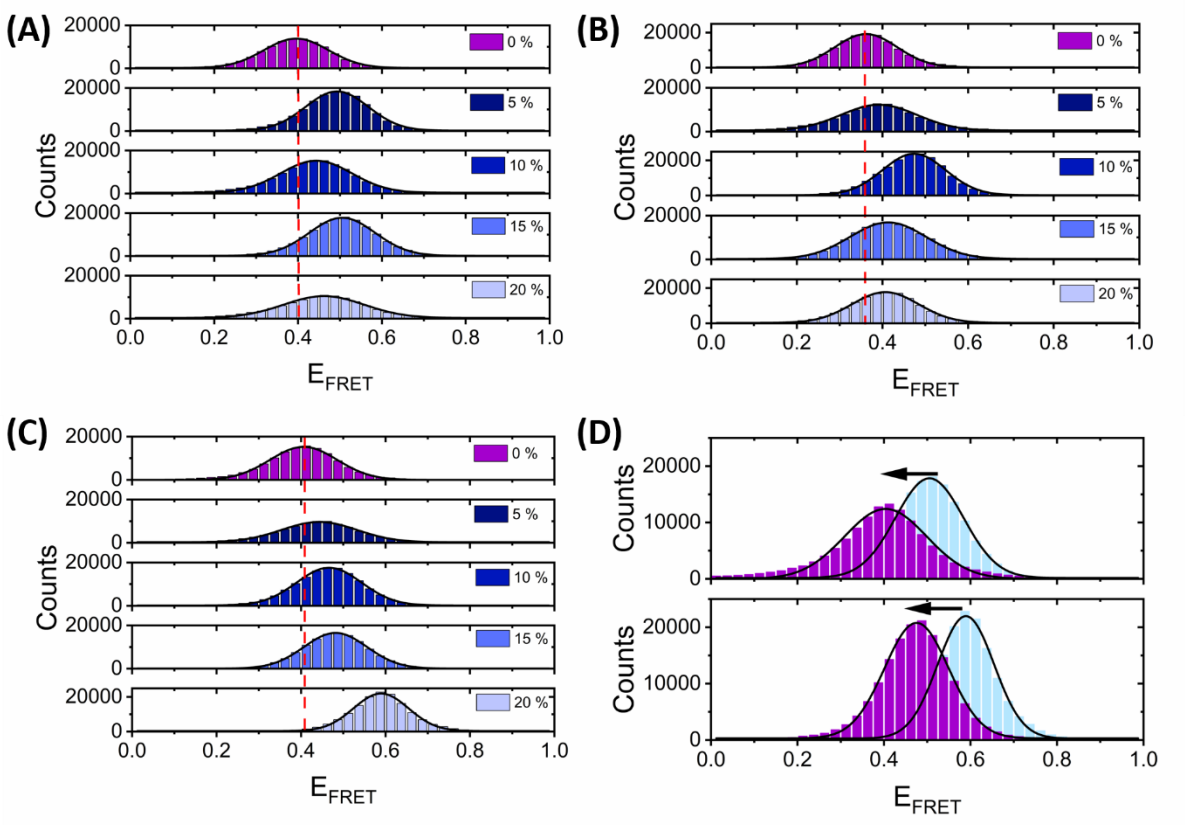

Figure 3. High molecular weight crowders induce reversible structural changes in single surface-tethered vesicles. Representative variations in the FRET efficiency histograms obtained for *N* > 2,000 vesicles in the absence and presence of (A) PEG400, (B) Ficol400 and (C) PEG8000 at 5 %, 10 %, 15 % and 20 % (*w/V*) in 50 mM Tris buffer (pH 8). The dashed red lines correspond to the peak positions of the FRET efficiency histograms obtained in the absence of crowder. Solid black lines represent

Gaussian fits. (D) FRET efficiency histograms obtained from N > 2,000 vesicles in the presence of PEG400 (blue, top panel) and PEG8000 (blue, lower panel) and after vigorous washing of the sample with 50 mM Tris (pH 8) buffer (purple).

A direct quantitative comparison between the effects of molecular crowding seen here on highly curved LUVs and previous work on GUVs is not entirely straightforward for a number of factors. For instance, the optical imaging of GUVs encapsulating molecular crowders as performed previously[32] only reports on macroscopic changes from a cross-sectional slice across the vesicles. In contrast, the smFRET approach described here provides access to the mean dye separation distance across the entire three-dimensional volume of the vesicle. Nevertheless, both sets of vesicles undergo rapid and substantial morphological changes in response to molecular crowders at similar concentrations. Thus, our smFRET work on sub-micron sized vesicles is complementary to the optical imaging of GUVs, with both datasets suggesting membrane conformation is substantially altered in response to molecular crowding.

Conclusion

The major findings of this work can be summarized as follows: (i) inclusion of the low molecular weight crowding agent sorbitol, and the high molecular weight crowders PEG400, Ficoll400 and PEG8000 all induce morphological changes in single highly-curved lipid vesicles, (ii) the morphological changes can be assigned to a global compaction of the vesicle structure, and (iii) crowding by sorbitol leads to permanent vesicle compaction whereas crowding by the high molecular weight polymers leads to reversible morphological changes. These results have emerged not from a standalone tool, but from the combination of ensemble and time-resolved FRET measurements, dynamic light scattering, electron microscopy and the imaging of single-vesicles using methods capable of overcoming the optical diffraction limit. It can be seen that under all conditions tested, the compaction of large unilamellar vesicles is achieved by only modest concentrations of crowder, and while it is generally thought that high molecular weight crowders induce morphological changes by the excluded volume effect[23, 52-54], the irreversible nature of the sorbitol-induced compaction points towards a specific and permanent crowder-lipid interaction within the intact bilayer. These results may thus have general implications for not only understanding the effect of molecular crowding on membrane-bound compartments, including highly curved exosomes and vesicles implicated in trafficking pathways, but also for the precise control and switching of vesicle conformation *in vitro*.

Acknowledgements

S. D. Q. acknowledges support from Alzheimer's Research UK (RF2019-A-001). This study was also supported by BBSRC (BB/W000555/1) and the Leverhulme Trust (RPG-2019-156). We thank Prof. Daniella Barilla (Department of Biology, University of York, UK) for use of DLS instrumentation, Prof. Thomas Krauss (Department of Physics, University of York, UK) for use of SEM Nanocentre facilities, the Bioscience Technology Facility (Department of Biology, University of York, UK) for use of fluorescence spectroscopy apparatus and Prof. Marco Fritzsche (University of Oxford, UK) for the donation of FliptR.

References

1. Chan, Y. H. M.; Boxer, S. G. Model Membrane Systems and Their Applications. *Current Opinion in Chemical Biology* **2007,** *11* (6), 581-587.
2. Zong, W.; Shao, X. T.; Chai, Y. H.; Wang, X. W.; Han, S.; Chu, H. T.; Zhu, C. T.; Zhang, X. A. Liposomes Encapsulating Artificial Cytosol as Drug Delivery System. *Biophys Chem* **2022,** *281*.

3. Torchilin, V. P. Recent Advances with Liposomes as Pharmaceutical Carriers. *Nat Rev Drug Discov* **2005,** *4* (2), 145-160.
4. Okumus, B.; Arslan, S.; Fengler, S. M.; Myong, S.; Ha, T. Single Molecule Nanocontainers Made Porous Using a Bacterial Toxin. *J Am Chem Soc* **2009,** *131* (41), 14844-14849.
5. Stengel, G.; Zahn, R.; Hook, F. DNA-Induced Programmable Fusion of Phospholipid Vesicles (Vol 129, Pg 9584, 2007). *J Am Chem Soc* **2008,** *130* (7), 2372-2372.
6. Mora, N. L.; Boyle, A. L.; van Kolck, B. J.; Rossen, A.; Pokorna, S.; Koukalova, A.; Sachl, R.; Hof, M.; Kros, A. Controlled Peptide-Mediated Vesicle Fusion Assessed by Simultaneous Dual-Colour Time-Lapsed Fluorescence Microscopy. *Sci Rep-Uk* **2020,** *10* (1).
7. Diao, J. J.; Ishitsuka, Y.; Lee, H.; Joo, C.; Su, Z. L.; Syed, S.; Shin, Y. K.; Yoon, T. Y.; Ha, T. A Single Vesicle-Vesicle Fusion Assay for in Vitro Studies of Snares and Accessory Proteins. *Nat Protoc* **2012,** *7* (5), 921-934.
8. Dalgarno, P. A.; Juan-Colas, J.; Hedley, G. J.; Pineiro, L.; Novo, M.; Perez-Gonzalez, C.; Samuel, I. D. W.; Leake, M. C.; Johnson, S.; Al-Soufi, W.; Penedo, J. C.; Quinn, S. D. Unveiling the Multi-Step Solubilization Mechanism of Sub-Micron Size Vesicles by Detergents. *Sci Rep-Uk* **2019,** *9*.
9. Juan-Colas, J.; Dresser, L.; Morris, K.; Lagadou, H.; Ward, R. H.; Burns, A.; Tear, S.; Johnson, S.; Leake, M. C.; Quinn, S. D. The Mechanism of Vesicle Solubilization by the Detergent Sodium Dodecyl Sulfate. *Langmuir* **2020,** *36* (39), 11499-11507.
10. Anandan, A.; Vrielink, A. Detergents in Membrane Protein Purification and Crystallisation. *Adv Exp Med Biol* **2016,** *922*, 13-28.
11. Model, M. A.; Hollembeak, J. E.; Kurokawa, M. Macromolecular Crowding: A Hidden Link between Cell Volume and Everything Else. *Cell Physiol Biochem* **2021,** *55* (S1), 25-40.
12. Zimmerman, S. B.; Minton, A. P. Macromolecular Crowding - Biochemical, Biophysical, and Physiological Consequences. *Annu Rev Bioph Biom* **1993,** *22*, 27-65.
13. Neuweiler, H.; Lollmann, M.; Doose, S.; Sauer, M. Dynamics of Unfolded Polypeptide Chains in Crowded Environment Studied by Fluorescence Correlation Spectroscopy. *J Mol Biol* **2007,** *365* (3), 856-869.
14. Soranno, A.; Koenig, I.; Borgia, M. B.; Hofmann, H.; Zosel, F.; Nettels, D.; Schuler, B. Single-Molecule Spectroscopy Reveals Polymer Effects of Disordered Proteins in Crowded Environments. *P Natl Acad Sci USA* **2014,** *111* (13), 4874-4879.
15. Baltierra-Jasso, L. E.; Morten, M. J.; Laflor, L.; Quinn, S. D.; Magennis, S. W. Crowding-Induced Hybridization of Single DNA Hairpins. *J Am Chem Soc* **2015,** *137* (51), 16020-16023.
16. Dupuis, N. F.; Holmstrom, E. D.; Nesbitt, D. J. Molecular-Crowding Effects on Single-Molecule Rna Folding/Unfolding Thermodynamics and Kinetics. *P Natl Acad Sci USA* **2014,** *111* (23), 8464-8469.
17. Holmstrom, E. D.; Dupuis, N. F.; Nesbitt, D. J. Kinetic and Thermodynamic Origins of Osmolyte-Influenced Nucleic Acid Folding. *J Phys Chem B* **2015,** *119* (9), 3687-3696.
18. Minton, A. P. Models for Excluded Volume Interaction between an Unfolded Protein and Rigid Macromolecular Cosolutes: Macromolecular Crowding and Protein Stability Revisited. *Biophys J* **2005,** *88* (2), 971-985.
19. Sarkar, M.; Smith, A. E.; Pielak, G. J. Impact of Reconstituted Cytosol on Protein Stability. *P Natl Acad Sci USA* **2013,** *110* (48), 19342-19347.
20. Dix, J. A.; Verkman, A. S. Crowding Effects on Diffusion in Solutions and Cells. *Annu Rev Biophys* **2008,** *37*, 247-263.
21. Keating, C. D. Aqueous Phase Separation as a Possible Route to Compartmentalization of Biological Molecules. *Accounts Chem Res* **2012,** *45* (12), 2114-2124.
22. van den Berg, J.; Boersma, A. J.; Poolman, B. Microorganisms Maintain Crowding Homeostasis. *Nat Rev Microbiol* **2017,** *15* (5), 309-318.
23. Sung, H. L.; Sengupta, A.; Nesbitt, D. Smaller Molecules Crowd Better: Crowder Size Dependence Revealed by Single-Molecule Fret Studies and Depletion Force Modeling Analysis. *J Chem Phys* **2021,** *154* (15).

24. Culik, R. M.; Abaskharon, R. M.; Pazos, I. M.; Gai, F. Experimental Validation of the Role of Trifluoroethanol as a Nanocrowder. *J Phys Chem B* **2014,** *118* (39), 11455-11461.
25. Money, N. P. Osmotic Pressure of Aqueous Polyethylene Glycols : Relationship between Molecular Weight and Vapor Pressure Deficit. *Plant Physiol* **1989,** *91* (2), 766-9.
26. Parsegian, V. A.; Rand, R. P.; Rau, D. C. Osmotic Stress, Crowding, Preferential Hydration, and Binding: A Comparison of Perspectives. *P Natl Acad Sci USA* **2000,** *97* (8), 3987-3992.
27. Lentz, B. R. Polymer-Induced Membrane-Fusion - Potential Mechanism and Relation to Cell-Fusion Events. *Chem Phys Lipids* **1994,** *73* (1-2), 91-106.
28. Kuhl, T.; Guo, Y. Q.; Alderfer, J. L.; Berman, A. D.; Leckband, D.; Israelachvili, J.; Hui, S. W. Direct Measurement of Polyethylene Glycol Induced Depletion Attraction between Lipid Bilayers. *Langmuir* **1996,** *12* (12), 3003-3014.
29. Chen, I. A.; Roberts, R. W.; Szostak, J. W. The Emergence of Competition between Model Protocells. *Science* **2004,** *305* (5689), 1474-1476.
30. Terasawa, H.; Nishimura, K.; Suzuki, H.; Matsuura, T.; Yomo, T. Coupling of the Fusion and Budding of Giant Phospholipid Vesicles Containing Macromolecules. *P Natl Acad Sci USA* **2012,** *109* (16), 5942-5947.
31. Lehtonen, J. Y. A.; Kinnunen, P. K. J. Poly(Ethylene Glycol)-Induced and Temperature-Dependent Phase-Separation in Fluid Binary Phospholipid-Membranes. *Biophys J* **1995,** *68* (2), 525-535.
32. Su, W. C.; Gettel, D. L.; Chabanon, M.; Rangamani, P.; Parikh, A. N. Pulsatile Gating of Giant Vesicles Containing Macromolecular Crowding Agents Induced by Colligative Nonideality. *J Am Chem Soc* **2018,** *140* (2), 691-699.
33. Yadav, J. K. Macromolecular Crowding Enhances Catalytic Efficiency and Stability of Alpha-Amylase. *ISRN Biotechnol* **2013,** *2013*, 737805.
34. Stetefeld, J.; McKenna, S. A.; Patel, T. R. Dynamic Light Scattering: A Practical Guide and Applications in Biomedical Sciences. *Biophys Rev* **2016,** *8* (4), 409-427.
35. Conteduca, D.; Quinn, S. D.; Krauss, T. F. Dielectric Metasurface for High-Precision Detection of Large Unilamellar Vesicles. *J Optics-Uk* **2021,** *23* (11).
36. Preus, S.; Noer, S. L.; Hildebrandt, L. L.; Gudnason, D.; Birkedal, V. Isms: Single-Molecule Fret Microscopy Software. *Nat Methods* **2015,** *12* (7), 593-4.
37. Garenne, D.; Libchaber, A.; Noireaux, V. Membrane Molecular Crowding Enhances Mreb Polymerization to Shape Synthetic Cells from Spheres to Rods. *P Natl Acad Sci USA* **2020,** *117* (4), 1902-1909.
38. Khodadadi, S.; Clark, N. J.; McAuley, A.; Cristiglio, V.; Curtis, J. E.; Shalaev, E. Y.; Krueger, S. Influence of Sorbitol on Protein Crowding in Solution and Freeze-Concentrated Phases. *Soft Matter* **2014,** *10* (23), 4056-4060.
39. Sukenik, S.; Sapir, L.; Harries, D. Osmolyte Induced Changes in Peptide Conformational Ensemble Correlate with Slower Amyloid Aggregation: A Coarse-Grained Simulation Study. *J Chem Theory Comput* **2015,** *11* (12), 5918-5928.
40. Sukenik, S.; Politi, R.; Ziserman, L.; Danino, D.; Friedler, A.; Harries, D. Crowding Alone Cannot Account for Cosolute Effect on Amyloid Aggregation. *Plos One* **2011,** *6* (1).
41. Richter, K.; Nessling, M.; Lichter, P. Experimental Evidence for the Influence of Molecular Crowding on Nuclear Architecture. *J Cell Sci* **2007,** *120* (9), 1673-1680.
42. Colom, A.; Derivery, E.; Soleimanpour, S.; Tomba, C.; Molin, M. D.; Sakai, N.; Gonzalez-Gaitan, M.; Matile, S.; Roux, A. A Fluorescent Membrane Tension Probe. *Nat Chem* **2018,** *10* (11), 1118-1125.
43. Drab, M.; Pandur, Z.; Penic, S.; Iglic, A.; Kralj-Iglic, V.; Stopar, D. A Monte Carlo Study of Giant Vesicle Morphologies in Nonequilibrium Environments. *Biophys J* **2021,** *120* (20), 4418-4428.
44. Jurkiewicz, P.; Cwiklik, L.; Vojtiskova, A.; Jungwirth, P.; Hof, M. Structure, Dynamics, and Hydration of Popc/Pops Bilayers Suspended in Nacl, Kcl, and Cscl Solutions. *Bba-Biomembranes* **2012,** *1818* (3), 609-616.

45. Dresser, L.; Hunter, P.; Yendybayeva, F.; Hargreaves, A. L.; Howard, J. A. L.; Evans, G. J. O.; Leake, M. C.; Quinn, S. D. Amyloid-Beta Oligomerization Monitored by Single-Molecule Stepwise Photobleaching. *Methods* **2021,** *193*, 80-95.
46. Kunding, A. H.; Mortensen, M. W.; Christensen, S. M.; Stamou, D. A Fluorescence-Based Technique to Construct Size Distributions from Single-Object Measurements: Application to the Extrusion of Lipid Vesicles. *Biophys J* **2008,** *95* (3), 1176-1188.
47. Balomenos, A. D.; Stefanou, V.; Manolakos, E. S. Analytics and Visualization Tools to Characterize Single-Cell Stochasticity Using Bacterial Single-Cell Movie Cytometry Data. *Bmc Bioinformatics* **2021,** *22* (1).
48. Kaur, T.; Alshareedah, I.; Wang, W.; Ngo, J.; Moosa, M. M.; Banerjee, P. R. Molecular Crowding Tunes Material States of Ribonucleoprotein Condensates. *Biomolecules* **2019,** *9* (2).
49. Paudel, B. P.; Fiorini, E.; Borner, R.; Sigel, R. K. O.; Rueda, D. S. Optimal Molecular Crowding Accelerates Group Ii Intron Folding and Maximizes Catalysis. *P Natl Acad Sci USA* **2018,** *115* (47), 11917-11922.
50. Banerjee, P. R.; Moosa, M. M.; Deniz, A. A. Two-Dimensional Crowding Uncovers a Hidden Conformation of Alpha-Synuclein. *Angew Chem Int Edit* **2016,** *55* (41), 12789-12792.
51. Junker, N. O.; Vaghefikia, F.; Albarghash, A.; Hofig, H.; Kempe, D.; Walter, J.; Otten, J.; Pohl, M.; Katranidis, A.; Wiegand, S.; Fitter, J. Impact of Molecular Crowding on Translational Mobility and Conformational Properties of Biological Macromolecules. *J Phys Chem B* **2019,** *123* (21), 4477-4486.
52. Kilburn, D.; Roh, J. H.; Guo, L.; Briber, R. M.; Woodson, S. A. Molecular Crowding Stabilizes Folded Rna Structure by the Excluded Volume Effect. *J Am Chem Soc* **2010,** *132* (25), 8690-8696.
53. Minton, A. P. Excluded Volume as a Determinant of Macromolecular Structure and Reactivity. *Biopolymers* **1981,** *20* (10), 2093-2120.
54. Minton, A. P. The Influence of Macromolecular Crowding and Macromolecular Confinement on Biochemical Reactions in Physiological Media. *J Biol Chem* **2001,** *276* (14), 10577-10580.
55. Dresser, L.; Graham, S. P.; Miller, L. M.; Conteduca, D., Johnson, S.; Leake, M. C.; Quinn, S. Tween-20 Induces the Structual Remoedling of Single Lipid Vesicles. J. Phys. Chem. Lett. (2022) *In Press.*

Crowding induced morphological changes of synthetic lipid vesicles determined using smFRET

Steven D. Quinn[1,2], Jack Shepherd[1], Lara Dresser[1], Sarah Graham[1] , Donato Conteduca[1] & Mark C. Leake[1,2,3]

[1]Department of Physics, University of York, York, UK. YO10 5DD.

[2]York Biomedical Research Institute, University of York, York, UK. YO10 5DD.

[3]Department of Biology, University of York, York, UK. YO10 5DD.

Correspondence to: mark.leake@york.ac.uk

SUPPORTING INFORMATION

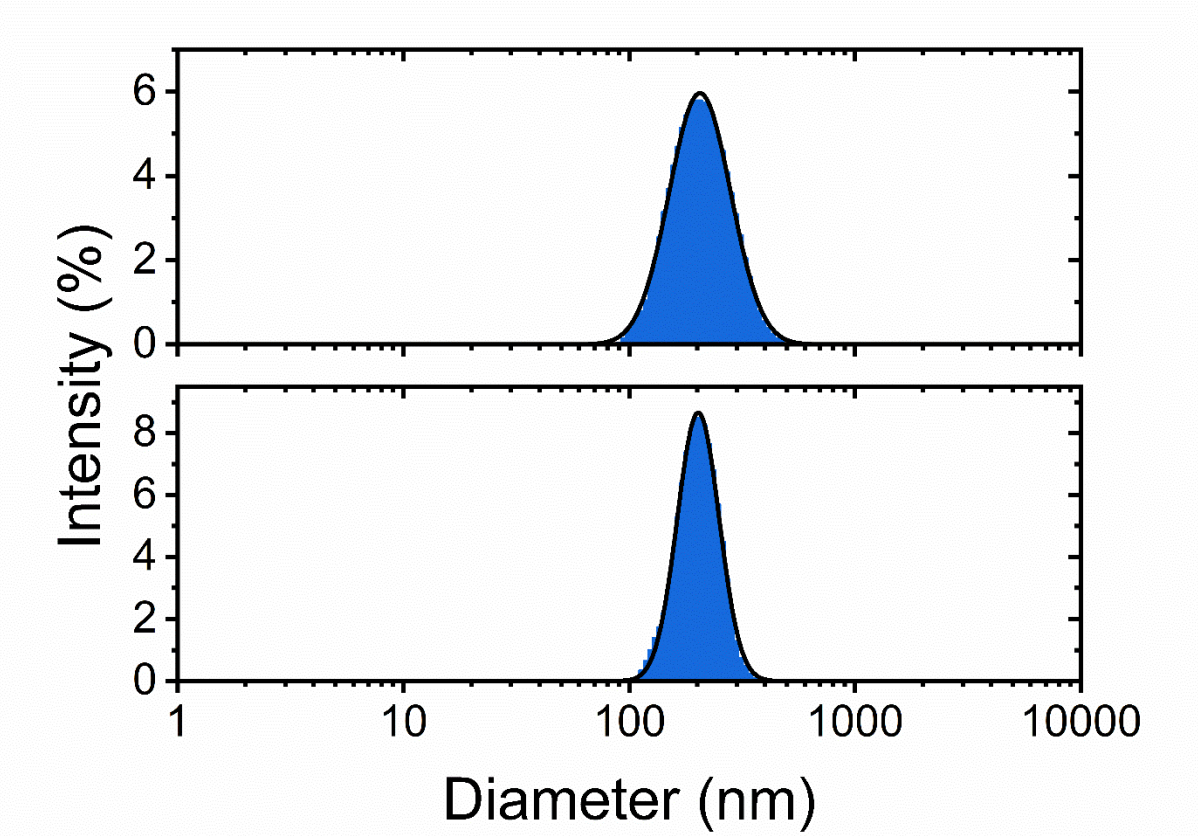

Figure S1. Representative DLS diameter distributions obtained from DiI and DiD loaded POPC vesicles (top panel) and unlabelled vesicles (bottom panel). Solution conditions: 50 mM Tris, pH 8.

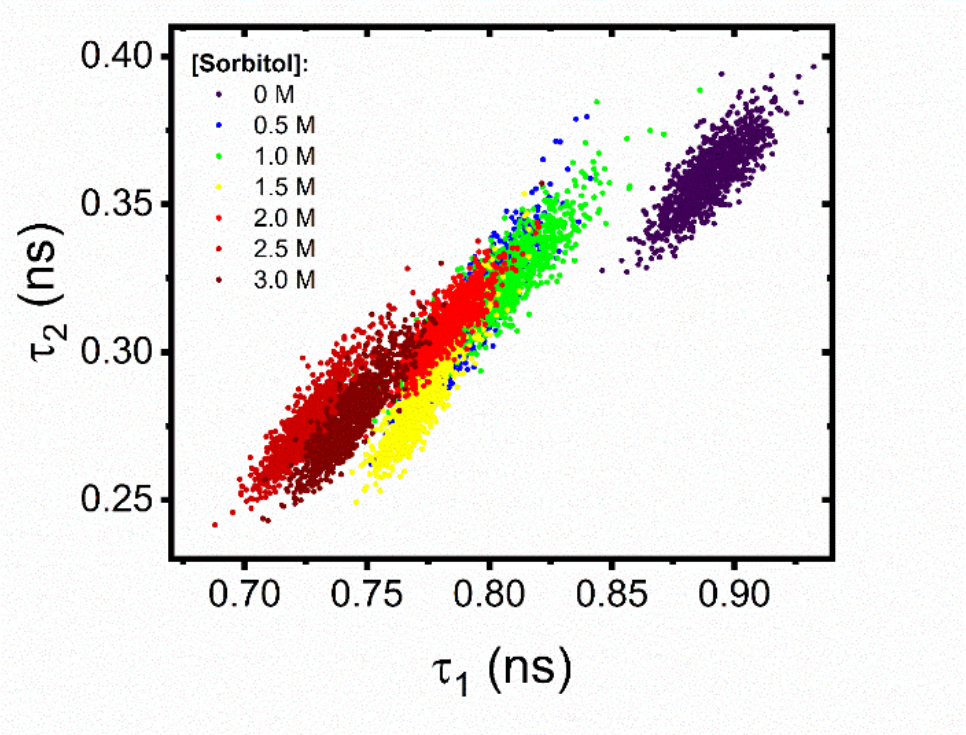

Figure S2. Representative variations in the lifetime components τ_1 and τ_2 extracted from DiI and DiD loaded POPC vesicles in the absence and presence of sorbitol.

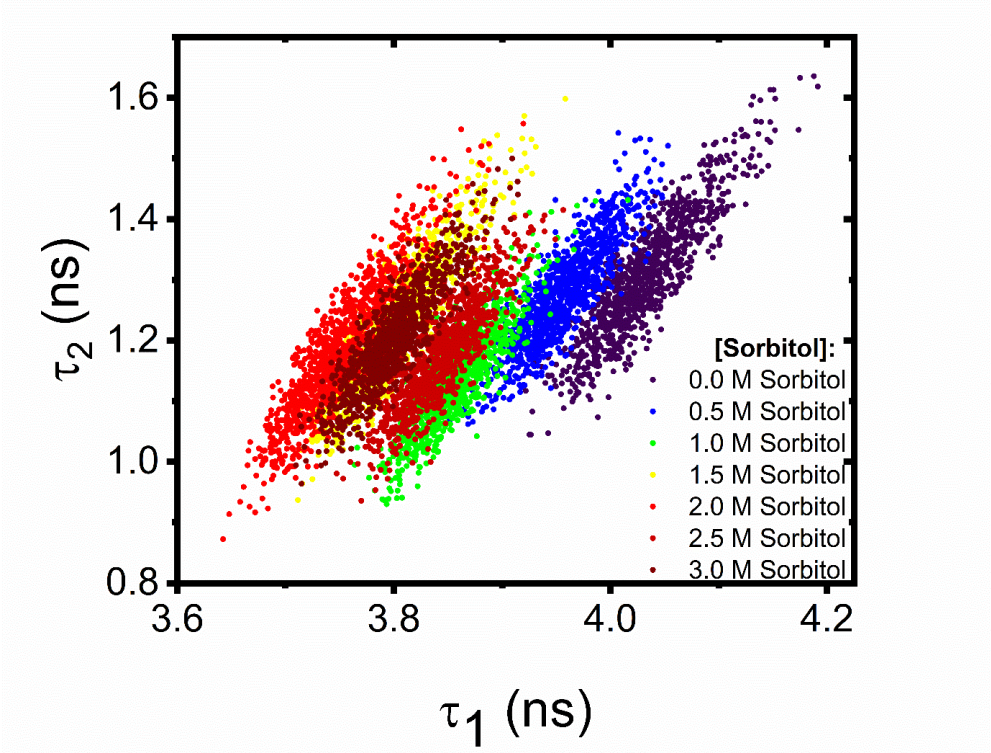

Figure S3. Representative variations in the lifetime components τ_1 and τ_2 extracted from FliptR loaded POPC vesicles in the absence and presence of sorbitol.

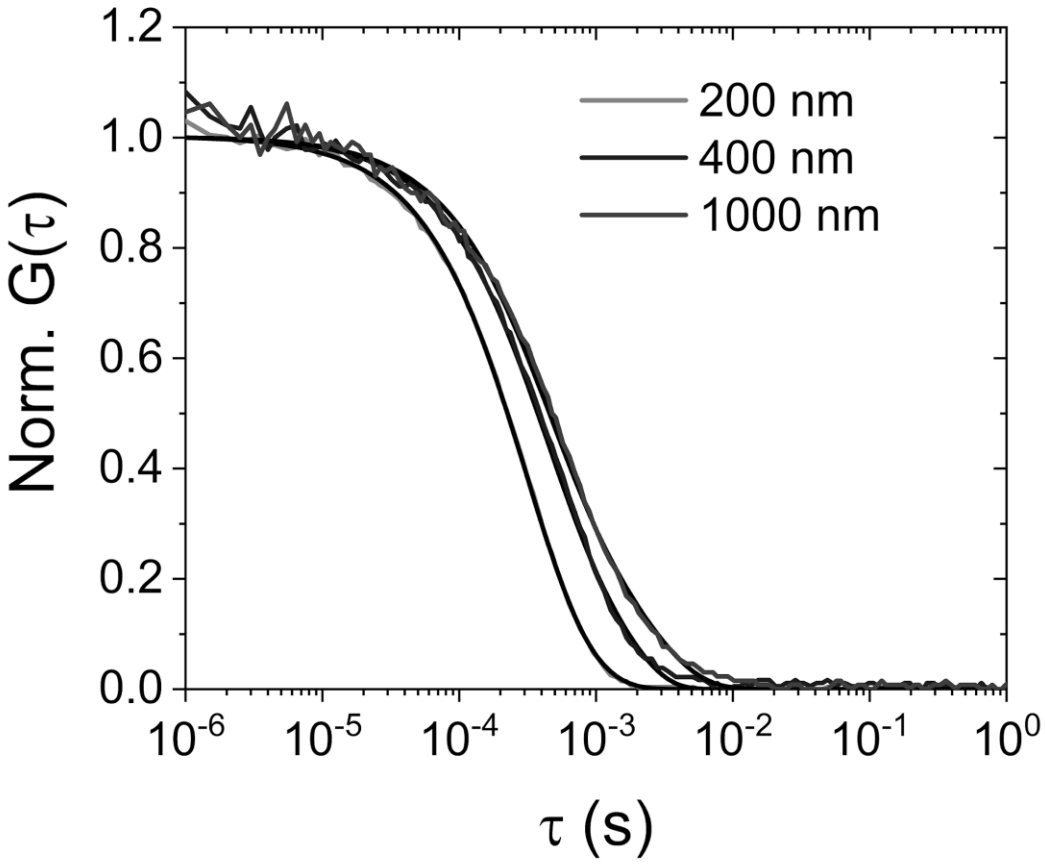

Figure S4. Representative variations in the normalized correlation curves obtained by DLS from DiI and DiD loaded POPC vesicles extruded through 200 nm (gra y), 400 nm (blue) and 1000 nm (red) pore diameter polycarbonate membrane filters. Solid black lines represent fits as describe in the Methods Section. Solution conditions: 50 mM Tris, pH 8.

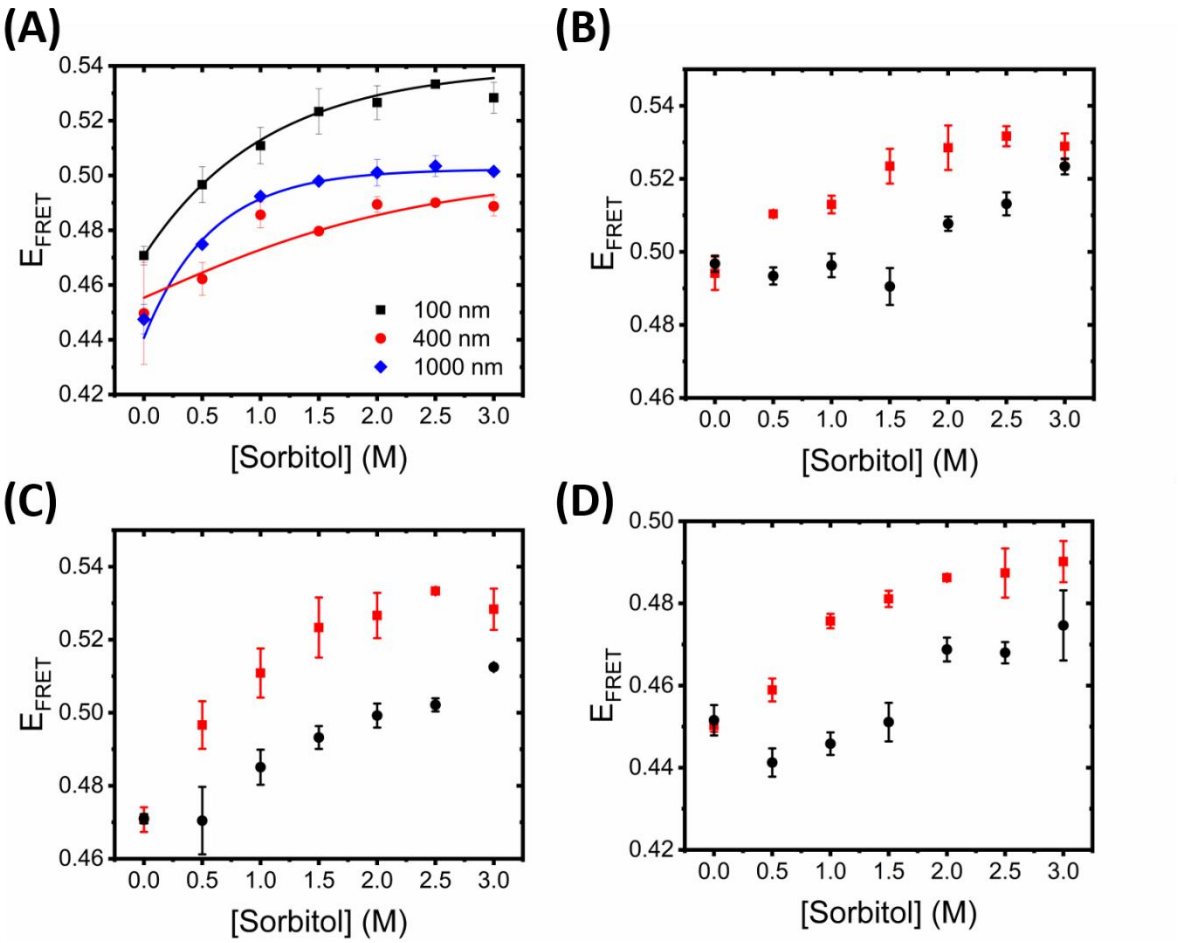

Figure S5. (A) Representative variation in E_{FRET} as a function of vesicle size. Also shown are E_{FRET} variations obtained from 100 nm diameter POPC (red) and POPS (black) vesicles at (B) 4°C, (C) 21°C and (D) 37°C.

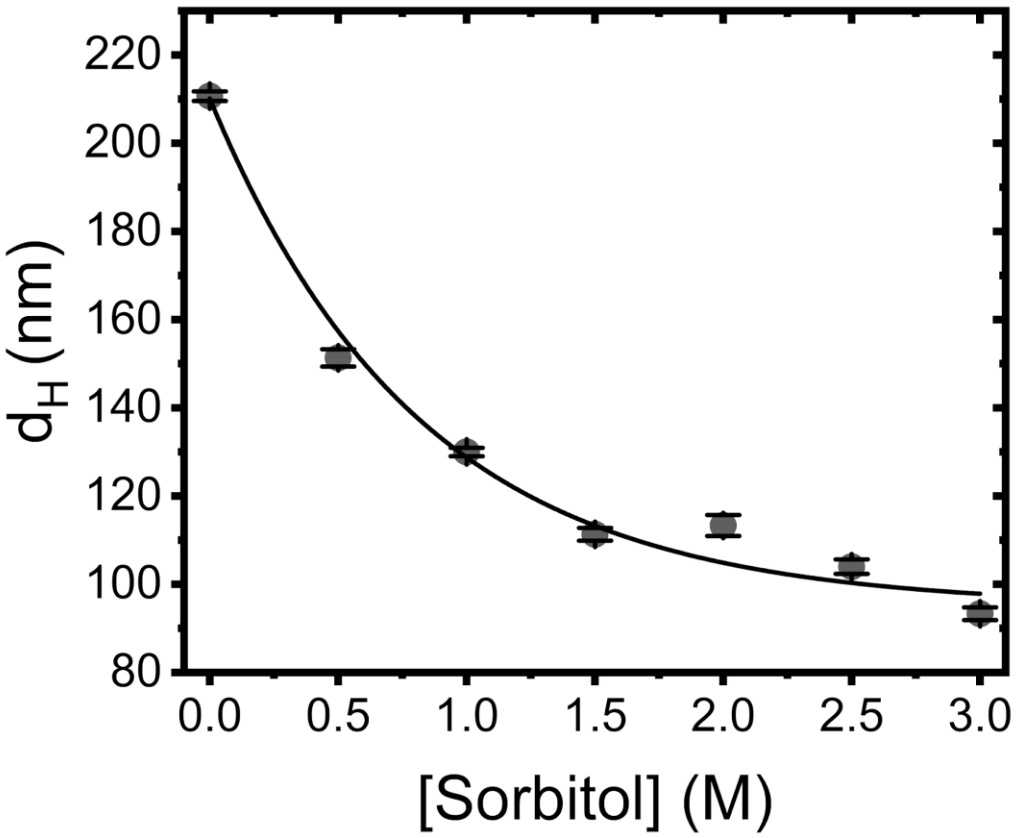

Figure S6. Variation in the mean hydrodynamic diameter of POPC-loaded LUVs under crowding conditions.